Available online at www.sciencedirect.com

ScienceDirect

journal homepage: www.intl.elsevierhealth.com/journals/dema

Effect of cooling protocol on mechanical properties and microstructure of dental veneering ceramics

Carina B. Tanaka[a], *Nur Hanani Binti Ahmad*[a], *Ayman Ellakwa*[b], *Jamie J. Kruzic*[a,*]

[a] *School of Mechanical and Manufacturing Engineering, UNSW Sydney, Sydney NSW 2052, Australia*
[b] *School of Dentistry, The University of Sydney, Westmead NSW 2145, Australia*

ARTICLE INFO

Article history:
Received 8 April 2019
Received in revised form
28 June 2019
Accepted 15 July 2019

Keywords:
Veneering ceramic
Dental restorative materials
Mechanical properties
Microstructure characterization
Cooling protocol

ABSTRACT

Objectives. Understand how cooling protocols control the microstructure and mechanical properties of veneering porcelains.

Methods. Two porcelain powders were selected, one used to veneer metallic frameworks (VM13) and one for zirconia frameworks (VM9). After the last firing cycle, the monolithic specimens were subjected to two cooling protocols: slow and fast. Flexural strength (FS) was evaluated by three-point beam bending and fracture toughness (K_{IC}) was evaluated by the single-edge V-notch beam (SEVNB) method. Scanning electron microscopy (SEM) was performed to determine the leucite crystal volume fraction (%), particle size, and matrix microcrack density. The results were compared by analysis of variances (ANOVA) and Tukey's multiple comparison test.

Results. The mechanical properties were significantly ($p < 0.05$) higher for the VM13 porcelain (FS = 111.0 MPa, K_{IC} = 1.01 MPa.$\sqrt{m}$) compared to VM9 (FS = 79.6 MPa, K_{IC} =0.87 MPa.$\sqrt{m}$) regardless of cooling protocol due to ~250% higher volume fraction of leucite crystals. The slow cooled VM13 and fast cooled VM9 resulted in the highest and lowest mechanical properties, respectively, while the VM9 slow cooled properties were similar to the VM13 fast cooled. The SEM revealed that the slow cooling significantly increased the volume fraction of leucite crystals by 33–41 %. Across both porcelains, a significant linear correlation between both mechanical properties (strength and toughness) and leucite crystal content was found. Slow cooling was also associated with increased crystal growth resulting in more matrix microcracking.

Significance. Controlled crystallization using slow cooling can be applied as a means of strengthening dental porcelains. However, the benefits of slow cooling may be partially offset by increasing the microcrack density in the glass matrix. To achieve the maximum benefit of slow cooling, it is recommending to develop heat treatments to produce porcelain with fine-grained and homogenously dispersed leucite crystals to achieve minimal glass matrix microcracking.

* *Corresponding author.*
E-mail address: j.kruzic@unsw.edu.au (J.J. Kruzic).
https://doi.org/10.1016/j.dental.2019.07.011

1. Introduction

Traditionally, the opaqueness of zirconia has been a limitation for dental restoration applications. High translucency is desired to allow light transmission through the restoration and impart a natural tooth-like appearance. Although the translucency of third generation dental zirconia ceramics has improved and is now comparable with lithium disilicate glass ceramics [1], there is still a large demand for enhanced aesthetics in anterior teeth requiring a veneering layer to mask the underlying zirconia framework.

A lower survival rate has been reported for veneered zirconia compared to porcelain-fused-to-metal (PFM) restorations [2]. The main cause of failure of veneered zirconia is chipping of the porcelain veneer, and this failure mode is rare in PFM restorations [3]. Damaged porcelain can significantly decrease the longevity of restorations, and replacement leads to an increased cost of restorative therapy. There are several factors thought to contribute to the high incidence of fracture for veneering porcelain in all-ceramic restorations. These include the low mechanical properties of dental porcelain [4,5], thermal expansion coefficient misfit of framework and veneering porcelain [6–8], and tensile residual stresses generated in the porcelain during cooling [9–11].

Porcelain is a heterogeneous multiphase material composed of crystalline leucite ($K_2O{\cdot}Al_2O_3{\cdot}4SiO_2$) embedded in a glassy matrix [12]. A key function of the leucite crystals is to help provide thermal compatibility between the veneering porcelain and the framework. In this regard, several studies have examined how the porcelain microstructure [13,14] and the coefficient of thermal expansion (CTE) [15,16] are affected by the various sintering and cooling protocols encountered during the fabrication of veneered restorations. While the glass phase provides the desired translucency, maintaining a larger amount of glass phase makes porcelains more susceptible to brittle fracture [17,18]. This is because another role of the leucite crystals is to reinforce and toughen the porcelain, primarily by crack deflection [19]. However, despite this reinforcement feldspathic porcelain is rarely used as monolithic restorative material due to its low mechanical properties, except in low load bearing areas and highly aesthetic regions of anterior teeth.

When considering the bilayer systems of veneered zirconia dental crowns, the CTE mismatch between the infrastructure (CTE≈10.5 ppm/K) and the veneering porcelain (CTE≈9.1 ppm/K) is thought to contribute to the fracture of veneered zirconia restoration due to the thermal residual stress generated between layers [6,8,9]. Because of this, slow cooling protocols have been recommended to reduce the amount of residual tensile stress generated in the porcelain veneer layer due to the CTE mismatch. The slow cooling allows time for the molecular rearrangement of the feldspathic porcelain and stress relaxation [7,20,21]. Slow cooling procedures have been shown to reduce the amount of residual thermal stresses [11,22,23] with the goal of reducing the occurrence of veneer chipping failures [24].

While many studies [5,11,25–30] have examined the effects of sintering and cooling protocols on bilayer specimens (veneer/framework), fewer studies [13,31] have been conducted to investigate the possible effects on the intrinsic porcelain mechanical properties independent of the residual stresses induced by the bilayer system. Tang et al. [13] focused only on the effect of multiple firings while Almeida et al. did not develop a description of how microstructure affects mechanical properties [31]. To the best of the authors' knowledge, there have been no studies examining the effect of cooling protocols on the microstructure and intrinsic mechanical properties of veneering porcelains. In the present work we hypothesize that a slower cooling protocol will induce larger amounts of leucite crystals and enhanced mechanical properties. Overall, it is thought that enhanced porcelain mechanical properties should lead to improved longevity of any veneered dental restoration.

Accordingly, this study examines the effects of cooling protocols on the mechanical properties and microstructure of veneering porcelains used both in PFM and veneered zirconia dental restorations. The motivation for using two different porcelains was to assess a wider range of leucite crystal content. The correlation between leucite crystal content and mechanical properties is explored, testing the hypothesis that the slow cooling protocol results in higher mechanical properties due to additional leucite crystals in the microstructure.

2. Material and methods

2.1. Specimen preparation

Two porcelain powders were selected, one used to veneer metallic frameworks (VM13, Vita-Zahnfabrik, Germany) and one for zirconia frameworks (VM9, Vita-Zahnfabrik, Germany). Monolithic bar-shaped specimens were prepared for fracture toughness (4 mm × 3 mm × 35 mm) and for flexural strength (1.5 mm × 2 mm × 25 mm) tests. The green bodies were prepared by mixing the porcelain powder with distilled water. The slurries were poured into a 3D printed resin mold (Form 2 printer with Grey Photoreactive Resin, Formlabs, Inc., USA), condensed using a dental plaster vibrator, and the excess water was removed by pressing with absorbent, lint free paper. For fracture toughness samples, a pre-notch was made in the green body by placing a razor blade in a groove on the 3 mm face of the mold.

The green-body specimens were sintered using a vacuum furnace (Programat CS2, Ivoclar Vivadent, USA) according to the manufacturer's instructions. The specimens were submitted to four firing cycles (Table 1) that simulates the multi-layering process to produce a veneered dental crown. After the glaze firing, the specimens were subjected to two different cooling protocols: slow and fast. For slow cooling the furnace was kept closed until the temperature reached 600 °C, while for the fast cooling protocol the furnace door was opened at the maximum firing temperature.

Unnotched specimens were hand-polished for the determination of flexural strength. Specimens were glued to a precision hand-polishing device (Accustop 30, Struers, Denmark) and sequentially ground and polished using progressively finer grit silicon carbide sandpapers (LaboPol-5, Struers, Denmark). The final surface finish was achieved using

Table 1 – Firing chart for veneering porcelain to zirconia and metal frameworks.

Firing	Veneering porcelain	Framework material	Pre-drying time (min)	Pre-Drying temperature (°C)	Heating rate (°C/min)	Maximum firing temperature (°C)	Holding time (min)
Washbake	VM9	Zirconia	2	500	55	950	1
	VM13	Metal	4	500	75	890	2
1° dentine	VM9	Zirconia	6	500	55	910	1
	VM13	Metal	6	500	55	880	1
2° dentine	VM9	Zirconia	6	500	55	900	1
	VM13	Metal	6	500	55	870	1
Glaze	VM9	Zirconia	0	500	80	900	1
	VM13	Metal	0	500	80	880	2

4000 grit sandpaper and the two long edges of the tensile surface were chamfered at 45°.

For fracture toughness samples, the molded notches were sharpened using a custom machine to slide a razor blade back-and-forth across the sample in the presence of 1 μm diamond paste (DP-Paste M, Struers, Denmark) and lubricant to produce a sharp V-notch radius of approximately 4.7 ± 1.5 μm, in accordance with ISO standard 23146 [32].

2.2. *Mechanical testing*

Flexural strength experiments were conducted on the unnotched beam specimens in general accordance with ASTM standard C1161 [33]. The specimens were loaded to fracture in a three-point bending fixture (span distance = 20 mm; roller diameter = 2.0 mm) at a cross-head speed of 1.0 mm/min using a computer controlled dynamic test machine (eXpert 5900 MTESTQuattro, ADMET, USA).

Flexural strength was calculated according to:

$$S = \frac{3PL}{2bd^2} \quad (1)$$

where P is the load at the fracture point, L is the length of the support span, and b and d are the specimen width and thickness, respectively. Fractured surfaces were platinum sputter coated and observed under a field-emission scanning electron microscope (SEM, FEI Nova NanoSEM 230, FEI Company, USA).

Fracture toughness was measured in terms of K_{IC} using the single-edge V-notch beam (SEVNB) method according to ISO standard 23146 [32]. The specimens were tested in a three-point bending test arrangement (roller span = 30 mm; roller diameter = 5 mm). Fracture toughness tests were conducted using a computer controlled dynamic test machine (eXpert 5900 MTESTQuattro, ADMET, USA) at a displacement rate of 0.5 mm/min until failure.

K_{IC} was calculated from the peak load at fracture according to the standard stress intensity factor equation for the SEVNB sample geometry:

$$K_I = \frac{PS}{BW^{3/2}} x \frac{3\left(\frac{a}{W}\right)^{1/2}\left[1.99 - \frac{a}{W}\left(1-\frac{a}{W}\right)\left\{2.15 - 3.93\left(\frac{a}{W}\right) + 2.7\left(\frac{a}{w}\right)^2\right\}\right]}{2\left(1+2\frac{a}{W}\right)\left(1-\frac{a}{W}\right)^{3/2}} \quad (2)$$

where P is the load at the fracture point, S is the length of the support span, a is the notch crack length, and B and W are the specimen thickness and width, respectively.

2.3. *Microstructural analysis*

The microstructure analyses were performed using the fractured SEVNB specimens. The 4 mm wide surfaces were polished with successively smaller grits down to 4000 grit and finished using a 0.05 μm alumina suspension (Buehler MasterPrep™). After polishing, the surfaces were etched with 9.6% hydrofluoric acid (HF) for 5 s and platinum sputter-coated for microstructural analysis by SEM.

Twenty SEM images (FEI Nova NanoSEM 230, FEI Company, USA) at a magnification of 4000x were used to determine the leucite crystal volume fraction (%) for each porcelain and cooling protocol and to evaluate the effect of the cooling protocol on the particle size for the VM9 material. The images were processed using the automated threshold method and the particle analyzer function in the software package ImageJ (ImageJ, National Institutes of Health, USA).

The particle size was obtained in terms of the surface diameter, d_s:

$$d_s = \sqrt{\frac{A_p}{\pi}}$$

where A_p is the particle surface area. The surface diameter assumes that the leucite particles, or clusters of particles, observed on the surface with area (A_p) represent the diameter of a spherical object having identical A_p [34].

The density of microcracks in the glass matrix was determined using quantitative stereology [35]. Horizontal grid lines were applied to the micrograph with 1 μm spacing using the grid analysis tool in ImageJ. Microcrack intersections with the test lines were counted manually on twenty micrographs for each group. The microcrack areal density (L_A = microcrack length per unit area) was calculated from the number of microcrack intersections with the length of lineal elements using the relationship:

$$L_A = \frac{\pi P_L}{2} \quad (3)$$

where P_L is the number of intersections per unit length of test line. The total number of counts per image was divided by the total length of test line (63 lines totaling 4608 μm in the scale of the micrograph) to obtain P_L.

2.4. Statistical analysis

The statistical significance of differences in flexural strength, fracture toughness, leucite crystal content, and microcrack density for the porcelains and cooling protocols was assessed using a two-way analysis of variances (ANOVA) in most cases. A one-way ANOVA was used for the particle surface diameter since only the VM9 porcelain was examined. Pair-wise comparisons were performed using Tukey's post-hoc test where $p < 0.05$ was considered statistically significant. The correlation between leucite crystal content and mechanical properties was investigated using Pearson correlation and a linear regression analysis.

3. Results

Flexural strength, fracture toughness, leucite crystal content, and glass matrix microcrack density results are shown in Table 2. The two-way ANOVA revealed that the mean flexural strength and fracture toughness were both significantly ($p < 0.05$) higher for the VM13 (FS = 111.0 MPa, K_{IC} = 1.01 MPa.$\sqrt{m}$) porcelain compared to VM9 (FS = 79.6 MPa, K_{IC} = 0.87 MPa.$\sqrt{m}$). The Tukey's pairwise comparisons showed that for the VM13 porcelain, slow cooling resulted in significantly higher flexural strength relative to fast cooling (Table 2). Furthermore, the mean strength of the VM9 porcelain was higher for the slow cooling protocol, but the difference was not statistically significant ($p > 0.05$) compared with fast cooling. While the fracture toughness followed an identical trend to the flexural strength (Table 2), only the fast cooled VM9 and the slow cooled VM13 showed a significant difference. Overall, the VM9 slow and VM13 fast cooled samples presented similar strength and toughness. The fast cooled VM9 porcelain presented the lowest mechanical properties.

Representative micrographs used for determining the leucite crystal content are shown in Fig. 1. The two-way ANOVA for leucite content revealed a significant effect of both material and cooling protocol, with a significant ($p = 0.02$) interaction. The significant interaction suggests that cooling protocol does not have the same magnitude effect across both materials. Tukey's post-hoc test showed that the leucite content was significantly different for each combination of material and cooling protocol (Table 2). The volume fraction of leucite was approximately 250% higher for VM13 compared to VM9, regardless of the cooling protocol. The slow cooling protocol increased the volume fraction of leucite by approximately 33–41 % compared to the fast-cooled groups (Table 2). Particle diameter was only measured for VM9 (Table 2). For VM13, the leucite crystals became more of a network and defining individual particles, or clusters, as spherical objects was not practical (Fig. 1). For VM9, the particle boundaries could be clearly identified since the leucite crystals were more dispersed within the glass matrix (Fig. 1).

The two-way ANOVA for microcrack density showed significantly ($p = 0.027$) higher microcrack density for the slow cooling protocol; however, Tukey's post-hoc test showed that there were no pair-wise differences between any of the groups. The two-way ANOVA also indicated that there was no significant difference between the porcelains and no significant interaction, which enabled the two materials to be grouped together for statistical comparison. This revealed significantly greater mean microcrack density for the slow cooled groups (7.4 mm/mm^2) compared with fast cooled ones (4.6 mm/mm^2). The one-way ANOVA for particle size showed that the mean surface diameter for VM9 slow cooled group was significantly higher ($p = 0.016$) compared with fast cooled.

The Pearson correlation coefficient showed a significant positive linear correlation between leucite crystal content and both the fracture toughness ($R^2 = 0.999$) and flexural strength ($R^2 = 0.984$) (Fig. 2). The p-value for fracture toughness ($p = 0.001$) and flexural strength ($p < 0.001$) indicate that the correlation is significant. As leucite crystal content increases, the mechanical properties also increase.

4. Discussion

The flexural strength of 74 MPa measured for the fast cooled VM9 in the present study is identical to the values of 74–76 MPa reported for various cooling protocols in Almeida et al. [31]. However, in contrast to that study, there is an apparent effect of slower cooling in increasing the strength to 85 MPa (Table 2), although it was not found to be statistically significant. Such results motivated the further analysis of microstructure to better understand how it is affected by the cooling protocol, and how it correlates to mechanical properties. And by studying VM13 in parallel, a wider range of microstructures was achieved.

The slow cooling protocol significantly increased the leucite crystal content both in VM9 and VM13 (Table 2 & Fig. 1), and the two-way ANOVA shows a significant effect of slower cooling rate increasing the flexural strength. Furthermore, there is a significant positive correlation for both the flexural strength and fracture toughness with leucite content across both materials (Fig. 2), and VM13 shows significantly higher flexural strength with slow cooling. This is attributed to the leucite acting as crystalline reinforcing phase within the glass matrix which increases the resistance to crack propagation by the crack deflection mechanism [19]. These factors together lead to the conclusion that slower cooling enhances leucite crystal content and mechanical properties of veneering porcelains.

The fact that differences in flexural strength for VM9 did not reach statistical significance in this, and in one previous study [31], may be explained by several possible factors. First, the significant increase in leucite crystal content with slow cooling is accompanied by a concomitant increase in microcrack density (Table 2). Microcracks are the result of the large CTE mismatch between the leucite (CTE = 22 ppm/°C) and the surrounding glass matrix (CTE = 8.6 ppm/°C) [36]. The CTE mismatch induces residual thermal stresses around and within the leucite crystals as a result of ~1.2% relative volume contraction of the leucite crystals that occurs during cooling [36]. These residual thermal stresses are partly relieved by the development of microcracks [19,37].

The density of microcracks in the glass matrix should also be related to the particle size. Although the stresses generated around the particles are independent of the particle size, particles must be above a critical size to have enough elastic

Table 2 – Means of fracture toughness, flexural strength, leucite crystal content, matrix microcrack density and particle size for two different veneering porcelains and cooling protocols.

Veneering Porcelain	Cooling protocol	Mean flexural strength (MPa)	Mean fracture toughness (MPa.$\sqrt{m}$)	Mean leucite crystal content (%)	Matrix microcrack density (mm/mm^2)	Mean particle surface diameter (μm)
VM9	Fast	74.3 ± 5.3^{C}	0.85 ± 0.12^{B}	10.7 ± 3.2^{D}	4.7 ± 4.1^{A}	2.9 ± 1.7^{B}
	Slow	85.0 ± 4.9^{BC}	0.88 ± 0.15^{AB}	15.1 ± 4.1^{C}	8.2 ± 4.2^{A}	3.3 ± 2.0^{A}
VM13	Fast	99.1 ± 14.0^{B}	0.98 ± 0.13^{AB}	27.8 ± 5.2^{B}	4.5 ± 4.8^{A}	–
	Slow	122.9 ± 25.5^{A}	1.04 ± 0.15^{A}	36.9 ± 5.1^{A}	6.7 ± 7.2^{A}	–

*Identical letters in the same column indicate no statistically significant difference ($p > 0.05$).

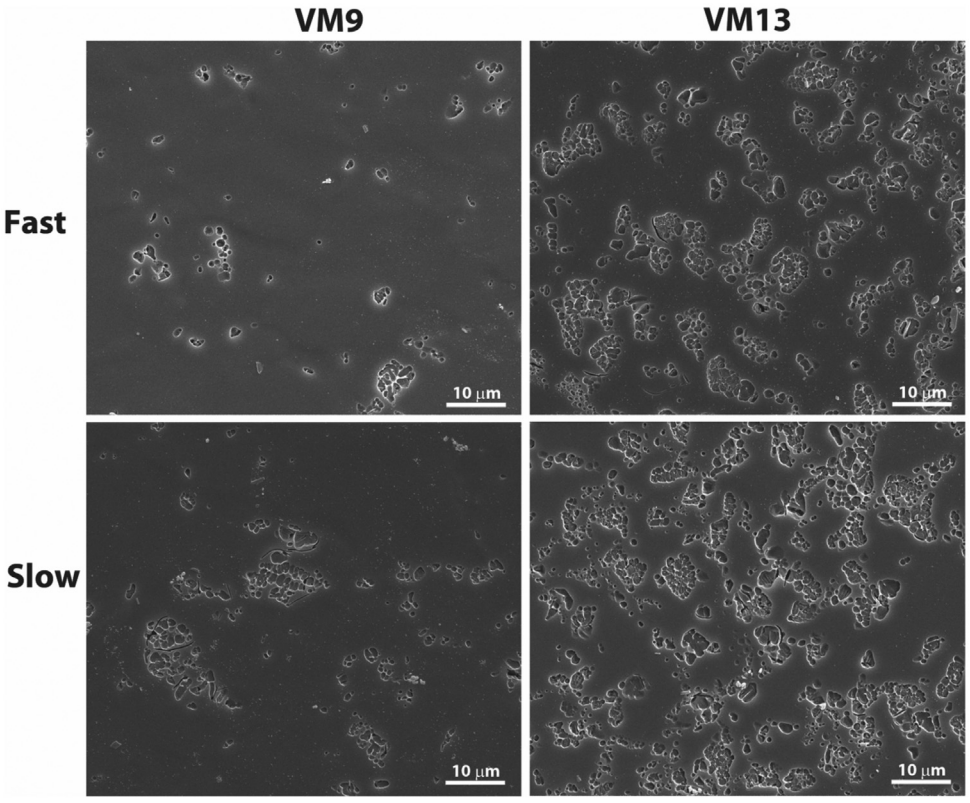

Fig. 1 – Micrographs of the VM9 and VM13 veneering porcelains subjected to slow and fast cooling protocols. Surfaces were etched with 9.6% hydrofluoric acid (HF) for 5 s.

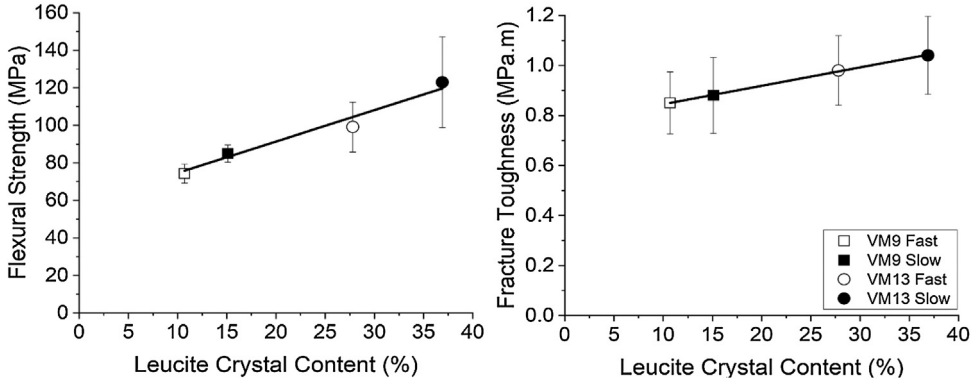

Fig. 2 – Plot of mechanical properties versus volume fraction of leucite crystal (left: flexural strength; right: fracture toughness) for the two veneering porcelains used. Data points indicate mean values, error bars indicate the standard deviation, and the line shows the best linear fit.

energy stored to initiate a crack and create two new surfaces [38]. Indeed, Mackert et al. [39] observed a higher frequency of microcracks around particles larger than 4 μm in diameter.

The leucite crystallization process that occurs upon slow cooling not only increases the number of crystals but also promotes crystal growth. The higher measured particle size for VM9 demonstrates that slow cooling caused more crystal growth than fast cooling (Table 2), which explains the significantly higher microcracking for slow cooling groups. Furthermore, in the later stages of cooling, the crystals may grow in a reduced glass viscosity matrix [40] at temperatures below the glass transition temperature, Tg. This limits the ability of the glass to relax stresses, further raising the stresses around the particles and in the glass matrix. While the particle sizes were only measured for the VM9 in the present study, it is noted that VM9 demonstrated larger microcracking density difference between slow and fast cooling and such measurements were important for explaining this difference with cooling protocol.

Microcracks can act as crack initiating stress concentrators that reduce the porcelain strength [39]. Accordingly, the higher amount of microcracks in the slow cooled porcelains may partially offset the benefit of the additional leucite crystals. The magnitude and significance of the role of microcracks is yet unclear and warrants further investigations. Next, it is clear from Fig. 1 that the distribution of the leucite crystals in VM9 is not homogeneous. Thus, while the slow cooled condition gives higher average leucite crystal content, the effectiveness of the crystals may be partially offset by the presence of relatively unreinforced glassy matrix regions that provide an easy crack path.

Overall, the results of this study suggest that additional crystallization of leucite should be an effective method to strengthen veneering porcelains, and perhaps reduce the propensity for chipping on zirconia frameworks, provided the benefit is not offset by other factors. If new cooling protocols are developed to achieve this, ideally the crystals should be fine grained [41,42] and uniformly distributed with minimal microcracking to achieve the maximum benefit.

While the nucleation and crystallization of leucite are difficult to control in highly viscous aluminosilicate glasses such as porcelain [43], a processing technique using a two-step sintering method combined with a heat treatment (>1100 °C for 1 h) has been shown to be effective at producing homogenous and fine-grained ($0.1 \pm 0.2\,\mu m^2$) leucite glass-ceramic [41]. However, for all ceramic bilayer systems, another consideration when annealing at such high temperatures will be avoiding undesirable phase transitions in the zirconium oxide framework that may degrade the properties [44].

The fracture toughness of 0.85 MPa$\sqrt{m}$ found for the fast cooled VM9 in the present study is somewhat lower than the values of 1.02–1.15 found in Almeida et al. [31]. However, this may be explained by the testing procedures. In the present work, the notches for the SEVNB samples were sharpened using a 1 μm diamond paste, while a 3 μm diamond paste was used in Almeida et al. [31]. The results to the SEVNB test can be sensitive to the notch root radius when the radius is above a critical size [45,46]. While the notch radii in Almeida et al. [31] were not reported, the finer abrasive used in the present study are expected to give a sharper final notch, and lower apparent fracture toughness. While it is unclear if the critical root radius was reached to give a minimum fracture toughness value that represents the true material property, the identical trends of flexural strength and fracture toughness with leucite crystal content are clear (Fig. 2) and further supports the above conclusions.

When considering the ideal cooling protocol for clinical applications, slow cooling will give more leucite crystals and improved mechanical properties in porcelains for both zirconia (VM9) and metal (VM13) frameworks. However, another key consideration is the effect of leucite crystals on the CTE mismatch. Increasing the crystal content is well known to increase the CTE of feldspathic porcelains [16]. A positive mismatch is desirable [30] to achieve compressive stresses in the veneer. For metal frameworks, the metal CTE is quite similar to the VM13 porcelain, ($\alpha_{metal} \sim 14.0$ ppm/°C verses $\alpha_{VM13} \sim 13.3$ ppm/°C) resulting in a positive mismatch of $\Delta\alpha \cong 0.7$ ppm/°C. Further increasing the VM13 leucite crystal content will push the CTE mismatch closer toward zero, or even negative. This is undesirable since CTE is a temperature dependent property and even with zero nominal mismatch at room temperature, the complex thermal firing history may result in tensile stresses in the veneering material [6] that would offset any strengthening benefit. On the other hand, the α mismatch between VM9 ($\alpha_{VM9} = 9.1$ ppm/°C) and Y-TZP ($\alpha_{Y\text{-}TZP} \sim 10.5$ ppm/°C) is nearly twice ($\Delta\alpha \cong 1.4$ ppm/°C) that for VM13 versus metal framework. Thus, compared to PFM restorations, there is more capacity to utilize slow cooling on Y-TZP frameworks to increase the mechanical properties of the veneer without producing unwanted tensile residual stresses that may occur as Δα approaches zero.

5. Conclusions

Based on a study on flexural strength, fracture toughness and microstructure analysis of two commercial dental porcelains, one used to veneer metallic frameworks and one for zirconia frameworks, the following conclusions can be made:

1 The superior mechanical properties of the slow cooled groups were attributed to the higher content of leucite crystals that better promoted crack deflection toughening mechanisms.
2 The improved mechanical properties of slow cooling are partially offset by the higher incidence of microcrack densities compared with fast cooled groups. The microcracks are attributed to the larger size of the crystals that results due to enhanced crystal growth during slow cooling.
3 Compared to the PFM veneering porcelain, slow cooling is better suited for enhancing the mechanical properties of the porcelain veneer used with zirconia-based framework since there is more capacity for increasing leucite crystal content while also maintaining a desirable CTE mismatch for all-ceramic bilayer systems.

Acknowledgements

The authors wish to thank Dr. Simon Hager for technical assistance and use of facilities supported by Microscopy Australia

at the Electron Microscope Unit at UNSW Sydney. The authors also thank Max Baerlocher for the dental laboratory support provided by Maxident Dental Technology, NSW, Australia.

REFERENCES

[1] Stawarczyk B, Keul C, Eichberger M, Figge D, Edelhoff D, Lumkemann N. Three generations of zirconia: from veneered to monolithic. Part I. Quintessence Int 2017;48:369–80.

[2] Pjetursson BE, Sailer I, Makarov NA, Zwahlen M, Thoma DS. All-ceramic or metal-ceramic tooth-supported fixed dental prostheses (FDPs)? A systematic review of the survival and complication rates. Part II: multiple-unit FDPs. Dent Mater 2015;31:624–39.

[3] Sailer I, Gottnerb J, Kanelb S, Hammerle CH. Randomized controlled clinical trial of zirconia-ceramic and metal-ceramic posterior fixed dental prostheses: a 3-year follow-up. Int J Prosthodont 2009;22:553–60.

[4] DeHoff PH, Barrett AA, Lee RB, Anusavice KJ. Thermal compatibility of dental ceramic systems using cylindrical and spherical geometries. Dent Mater 2008;24:744–52.

[5] Baldassarri M, Stappert CF, Wolff MS, Thompson VP, Zhang Y. Residual stresses in porcelain-veneered zirconia prostheses. Dent Mater 2012;28(8):873–9.

[6] Isgro G, Wang H, Kleverlaan CJ, Feilzer AJ. The effects of thermal mismatch and fabrication procedures on the deflection of layered all-ceramic discs. Dent Mater 2005;21:649–55.

[7] DeHoff PH, Anusavice KJ. Viscoelastic finite element stress analysis of the thermal compatibility of dental bilayer ceramic systems. Int J Prosthodont 2009;22: 56–61.

[8] Meira JBC, Reis BR, Tanaka CB, Ballester RY, Cesar PF, Versluis A, Swain MV. Residual stresses in Y-TZP crowns due to changes in the thermal contraction coefficient of veneers. Dent Mater 2013;29:594–601.

[9] Swain MV. Unstable cracking (chipping) of veneering porcelain on all-ceramic dental crowns and fixed partial dentures. Acta Biomater 2009;5:1668–77.

[10] Taskonak B, Mecholsky JJ, Anusavice KJ. Residual stresses in bilayer dental ceramics. Biomaterials 2005;26:3235–41.

[11] Tanaka CB, Harisha H, Baldassarri M, Wolff MS, Tong H, Meira JBC, Zhang Y. Experimental and finite element study of residual thermal stresses in veneered Y-TZP structures. Ceram Int 2016;42:9214–21.

[12] Christensen RP, Ploeger BJ. A clinical comparison of zirconia, metal and alumina fixed-prosthesis frameworks veneered with layered or pressed ceramic: a three-year report. J Am Dent Assoc 2010;141:1317–29.

[13] Tang X, Nakamura T, Usami H, Wakabayashi K, Yatani H. Effects of multiple firings on the mechanical properties and microstructure of veneering ceramics for zirconia frameworks. J Dent 2012;40:372–80.

[14] Mackert JR, Evans AL. Effect of cooling rate on leucite volume fraction in Dental Porcelains. J Dent Res 1991;70:137–9.

[15] Mackert JR, Butts MB, Fairhurst CW. The effect of the leucite transformation on dental porcelain expansion. Dent Mater 1986;2:32–6.

[16] Isgro G, Kleverlaan CJ, Wang H, Feilzer AJ. The influence of multiple firing on thermal contraction of ceramic materials used for the fabrication of layered all-ceramic dental restorations. Dent Mater 2005;21:557–64.

[17] Babu PJ, Alla RK, Alluri VR, Datla SR, Konakanchi A. Dental ceramics: Part I – An overview of composition, structure and properties. Am J Mater Eng Tech 2015;3:13–8.

[18] Yin L, Stoll R. 26 - ceramics in restorative dentistry A2 - low, I.M. Advances in ceramic matrix composites. Woodhead Publishing; 2014. p. 624–55.

[19] Cesar PF, Yoshimura HN, Miranda Júnior WG, Okada CY. Correlation between fracture toughness and leucite content in dental porcelains. J Dent 2005;33:721–9.

[20] Kim J, Dhital S, Zhivago P, Kaizer MR, Zhang Y. Viscoelastic finite element analysis of residual stresses in porcelain-veneered zirconia dental crowns. J Mech Behav Biomed Mater 2018;82:202–9.

[21] Taskonak B, Borges GA, Mecholsky Jr JJ, Anusavice KJ, Moore BK, Yan J. The effects of viscoelastic parameters on residual stress development in a zirconia/glass bilayer dental ceramic. Dent Mater 2008;24:1149–55.

[22] Belli R, Monteiro Jr S, Baratieri LN, Katte H, Petschelt A, Lohbauer U. A photoelastic assessment of residual stresses in zirconia-veneer crowns. J Dent Res 2012;91:316–20.

[23] Tholey MJ, Swain MV, Thiel N. Thermal gradients and residual stresses in veneered Y-TZP frameworks. Dent Mater 2011;27:1102–10.

[24] Paula VG, Lorenzoni FC, Bonfante EA, NRFA Silva, Thompson V, Bonfante G. Slow cooling protocol improves fatigue life of zirconia crowns. Dent Mater 2015;31:77–87.

[25] Benetti P, Kelly JR, Della Bona A. Analysis of thermal distributions in veneered zirconia and metal restorations during firing. Dent Mater 2013;29:1166–72.

[26] Al-Amleh B, Waddell JN, Lyons K, Swain MV. Influence of veneering porcelain thickness and cooling rate on residual stresses in zirconia molar crowns. Dent Mater 2014;30:271–80.

[27] Wendler M, Belli R, Petschelt A, Lohbauer U. Characterization of residual stresses in zirconia veneered bilayers assessed via sharp and blunt indentation. Dent Mater 2015;31:948–57.

[28] Mainjot AK, Schajer GS, Vanheusden AJ, Sadoun MJ. Influence of cooling rate on residual stress profile in veneering ceramic: measurement by hole-drilling. Dent Mater 2011;27:906–14.

[29] Benetti P, Kelly JR, Sanchez M, Della Bona A. Influence of thermal gradients on stress state of veneered restorations. Dent Mater 2014;30:554–63.

[30] Meirelles PD, Spigolon YO, Borba M, Benetti P. Leucite and cooling rate effect on porcelain-zirconia mechanical behavior. Dent Mater 2016;32:e382–8.

[31] Almeida Junior AAd, Longhini D, Suzuki PA, Ribeiro S, Santos C, Adabo GL. Effect of the cooling rate on the properties of veneer porcelain for zirconia dental prosthesis. Mater Res 2017;20:1418–24.

[32] ISO 23146. Fine ceramics (advanced ceramics, advanced technical ceramics) - Test methods for fracture toughness of monolithic ceramics - Single-edge-V-notch beam (SEVNB) method. ISO Geneva; 2012.

[33] ASTM C1161-13. Standard test method for flexural strength of advanced ceramics at ambient temperature. West Conshohocken, PA: ASTM International; 2013.

[34] Kowalczuk PB, Drzymala J. Physical meaning of the Sauter mean diameter of spherical particulate matter. Particul Sci Technol 2016;34:645–7.

[35] Underwood EE. Stereology, or the quantitative evaluation of microstructures. J Microsc-Oxford 1969;89:161–80.

[36] Denry IL, Mackert Jr JR, Holloway JA, Rosenstiel SF. Effect of cubic leucite stabilization on the flexural strength of feldspathic dental porcelain. J Dent Res 1996;75:1928–35.

[37] Mackert JR, Rueggeberg E, Lockwood PE, Evans AL, Thompson WO. Isothermal anneal effect on microcrack density around Leucite Particles in dental porcelain. J Dent Res 1994;73:1221–7.

[38] Davidge RW, Green TJ. The strength of two-phase ceramic/glass materials. J Mater Sci 1968;3:629–34.

[39] Mackert JR, Twiggs SW, Russell CM, Williams AL. Evidence of a critical leucite particle size for microcracking in dental porcelains. J Dent Res 2001;80:1574–9.
[40] Cattell MJ, Chadwick TC, Knowles JC, Clarke RL. The crystallization of an aluminosilicate glass in the K2O–Al2O3–SiO2 system. Dent Mater 2005;21:811–22.
[41] Cattell MJ, Chadwick TC, Knowles JC, Clarke RL, Samarawickrama DYD. The nucleation and crystallization of fine grained leucite glass-ceramics for dental applications. Dent Mater 2006;22:925–33.
[42] Chen X, Chadwick TC, Wilson RM, Hill R, Cattell MJ. Crystallization of high-strength fine-sized leucite glass-ceramics. J Dent Res 2010;89:1510–6.
[43] Greenwood GW, Greer AL, Herlach DM, Kelton KF, Höland W, Rheinberger V, Schweiger M. Control of nucleation in glass ceramics. Philosophical transactions of the royal society of London series a: mathematical. Phys Eng Sci 2003;361:575–89.
[44] Chevalier J, Gremillard L, Virkar AV, Clarke DR. The tetragonal-monoclinic transformation in zirconia: lessons learned and future trends. J Am Ceram Soc 2009;92:1901–20.
[45] Nishida T, Hanaki Y, Pezzotti G. Effect of notch-root radius on the fracture toughness of a fine-grained alumina. J Am Ceram Soc 1994;77:606–8.
[46] Damani R, Gstrein R, Danzer R. Critical notch-root radius effect in SENB-S fracture toughness testing. J Eur Ceram Soc 1996;16:695–702.